XPS, FTIR, EDX, and XRD analysis of Al_2O_3 scales grown on PM2000 alloy

Djebaili, K.; Mekhalif, Z.; Boumaza, A.; Djelloul, A.

Published in:
Journal of Spectroscopy

DOI:
10.1155/2015/868109

Publication date:
2015

Document Version
Publisher's PDF, also known as Version of record

Hindawi Publishing Corporation
Journal of Spectroscopy
Volume 2015, Article ID 868109, 16 pages
http://dx.doi.org/10.1155/2015/868109

Research Article

XPS, FTIR, EDX, and XRD Analysis of Al_2O_3 Scales Grown on PM2000 Alloy

K. Djebaili,[1] Z. Mekhalif,[2] A. Boumaza,[1] and A. Djelloul[1]

[1] *Structures, Properties and InterAtomic Interactions Laboratory (LASPI²A), Faculty of Science and Technology, University of Abbès Laghrour, 40000 Khenchela, Algeria*
[2] *Chemistry and Electrochemistry Surfaces Laboratory (LCES), Notre-Dame de la Paix Faculty, Road of Bruxelles 61, 5000 Namur, Belgium*

Correspondence should be addressed to A. Boumaza; charif_boumaza@yahoo.com

Received 18 January 2015; Revised 20 February 2015; Accepted 25 February 2015

Academic Editor: Djordje Mandrino

This work is an original example to compare the results obtained after calcination of Al_2O_3 hydroxides and oxidation of alumino-formers alloys. FTIR and XPS signatures were obtained for various oxidation temperatures and compared with those known from the literature about calcination of Al_2O_3 precursors. The aim of this work is to evaluate the use of IR spectroscopy and XPS analysis to probe the structural varieties of Al_2O_3. For this objective, a study of the PM2000 oxidation at various temperatures was conducted by means of XRD, IR spectroscopy, XPS analysis, EDX analysis, and SEM observations. This allowed us to clearly differentiate the transition Al_2O_3 from the α-Al_2O_3 and, amongst the transition Al_2O_3, to differentiate the characteristic of the IR spectrum of γ-δ phases from that of the θ phase.

1. Introduction

Most of the metallic materials functioning at high temperature need to have oxidation resistance. This resistance can be achieved when the chosen materials develop through oxidation, an oxide film which acts as a diffusion barrier while keeping a good adherence. Several studies have shown that the oxide layers as SiO_2, Cr_2O_3, and α-Al_2O_3 provide a satisfactory protective role, a protection based on the formation of a layer of α-Al_2O_3. Al_2O_3 is the most powerful principle. In this prospect, α-Al_2O_3 is a very good candidate. Before reaching the most stable Al_2O_3 [1], alumino-former materials developed transition Al_2O_3 among which the most common are γ, δ, and/or θ phases. Nowadays, it is not clear whether the growth of transition Al_2O_3 as a first step improves the protective properties of the further formed α-Al_2O_3 film. Moreover, one difficulty associated with the understanding of the influence of transition Al_2O_3 on the further oxidation resistance concerns the fact that, as mentioned in [2], the techniques which allow us to detect and characterize transition Al_2O_3 formed as thin layers (1 to 3 μm) are scarce and provide ambiguous answers. Indeed, the most common technique, the XRD, provides patterns for various Al_2O_3 which are relatively close to each other. Moreover, it seems that, in many cases, several transition phases can be simultaneously present [3]. In previous studies, transmission electron microscopy (TEM) was used to probe the oxidation of either an intermetallic alloy, Fe_3Al, or an ODS (oxide dispersion strengthening) FeCrAl alloy strengthened by very small Y_2O_3 particles, PM2000 [4–7]. The formation of transition Al_2O_3 for various heat treatment conditions was evidenced and the transition to the α-Al_2O_3 was studied. The formed oxide scales were characterized using analysis techniques such as scanning electron microscope (SEM), energy-dispersive X-ray spectroscopy (EDX), X-ray diffraction (XRD), Fourier transform infrared spectroscopy (FTIR), and X-ray photoelectron spectroscopy (XPS). The present study aims at examining whether FTIR and XPS analysis may provide a simple probe to various structural varieties of Al_2O_3 for applications of high temperature materials.

2. Experimental Techniques

2.1. Samples and Treatments. The Fe-based alloy PM2000 strengthened by oxide dispersion (ODS) received from

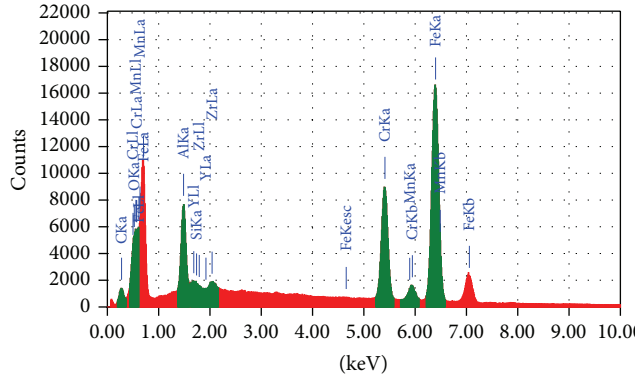

Figure 1: EDX analysis of the as-received PM2000.

Schwarzkopf Plansee was used; the chemical composition in weight percent is as follows: A1-5.0, Cr-22.0, Mn-0.2, C-0.02, Si-0.3, Y-0.1, Zr-0.1, and Fe-balance. Rectangular specimens of dimensions $1 \times 1\,\text{cm}^2$ and $1 \times 2\,\text{cm}^2$ and thickness of 1.0 ± 0.1 mm were sectioned. The oxidation of PM2000 alloy as a heat resistant material for high temperature applications was studied in air at 873, 973, 1073, 1173, 1273, 1373, and 1473 K according to the following heat treatment:

(i) heating it up to the specified temperature at 20 K/min;

(ii) maintaining it for 7 h at the oxidation temperature;

(iii) cooling it down rapidly to room temperature (air quench).

2.2. Characterization of Samples. All the samples were then characterized using XRD, SEM observations, EDX qualitative analysis, FTIR spectroscopy, and XPS spectroscopy.

(i) XRD analysis was performed with a PANalytical X'Pert ProMRD diffractometer with CuKa radiation ($\lambda = 0.15418$ nm). Data were collected with steps of 0.021° (2θ).

(ii) SEM images were taken on a field emission scanning microscope (JEOL 7500-F). The SEM used for the characterization is equipped by Genesis EDX spectroscopy system that was used to measure the composition of the elements constituting the films.

(iii) FTIR spectra were obtained using a Perkin-Elmer spectrometer at a resolution of $8\,\text{cm}^{-1}$. FTIR technique was used in the transmission mode in the $400–4000\,\text{cm}^{-1}$ range. For each sample, 120 scans were used. After oxidation, ~100 μg of the oxides was scraped. The oxide was then compressed together with 23 ± 2 mg of KBr in a cold 150 MPa isostatic press (CIP) in order to obtain a 200–250 μm thick pellet. All IR spectra are reporting absorbance ($A = -\log(I/I_0)$) as a function of the incident wavenumbers.

(iv) An XPS spectrometer was used to qualitatively and quantitatively verify the composition of the different powder compounds. The spectra were treated using the Thermo Advantage V5.27 software. The photoelectrons are excited using a monochromatic Al-Kα radiation as the excitation source, collected at $\theta = 0^\circ$ with respect to the surface normal and detected with a hemispherical analyzer. The spot size of the XPS source on the sample is 200 μm, and the analyzer is operated with a pass energy of 150 eV for the survey spectra and 20 eV for the accumulation spectra of the core levels. The pressure is maintained below 10^{-8} Torr during data collection, and the binding energies (Eb) of the obtained peaks are referenced to the C1s signal for C–H, which is set to 285.0 eV. XPS measurements are made with an uncertainty of about 0.1 eV to 0.2 eV.

2.3. SEM and EDX Analysis. For each tested temperature, oxidized specimens, contained in crucibles, were cooled to room temperature. For studies of scale morphology, composition, and crystal structure, EDX analysis was used. Figure 1 shows EDX analysis of the as-received PM2000, and the presence of the elements Fe, Cr, Al, Y, Zr, Si, Mn, and C is detected.

Significant differences in the scale morphology were observed by SEM, depending on the oxidation temperature. Both materials developed Al_2O_3 scales. Figure 2(a) shows nodules form during the early stages of oxidation; they consist of oxides enriched by Al, Fe, Cr, Si, or Mg. Fe/Cr oxides were detected for temperatures between 873 and 1073 K, and cracks and porosities are observed at 1073 K, as shown in Figure 2(b). Our observations are consistent with those in the literature [8–10]. In addition to α-Al_2O_3 (detected by XRD), Figure 2(c) shows metastable Al_2O_3 which is clearly observed at 1173 K, the so-called "platelet-like" oxide, and recognized to propagate by an outward Al anion diffusion in contrary to α-Al_2O_3 scale. The presence of this type of particles was correlated with the XRD analysis and they were assumed to be θ-Al_2O_3. It is well established [11, 12] that the growth rate of the metastable Al_2O_3 is of factor two to four times higher than the stable Al_2O_3, leading to faster Al consumption and as a result substantial decreasing of component's lifetime. The external surface of metastable oxide is very different from the equiaxed dense α-Al_2O_3 grains.

Table 1: Composition and stoichiometry of the thin films obtained by statistical analysis of EDX spectrum.

Element	(keV)	Atom%, PM2000, 873 K	Atom%, PM2000, 1073 K	Atom%, PM2000, 1173 K	Atom%, PM2000, 1473 K
C K	0.277	4	5	2	<1
O K	0.525	15	38	55	59
Mg K	1.253	<1	<1	<1	5
Al K	1.486	11	21	34	34
Si K	1.739	<1	<1	0	0
Cr K	5.411	17	9	3	<1
Fe K	6.398	52	26	5	<1
Y L	1.922			<1	0
Zr L	2.042				0
Al/O ratio		0.709	0.560	0.618	0.578

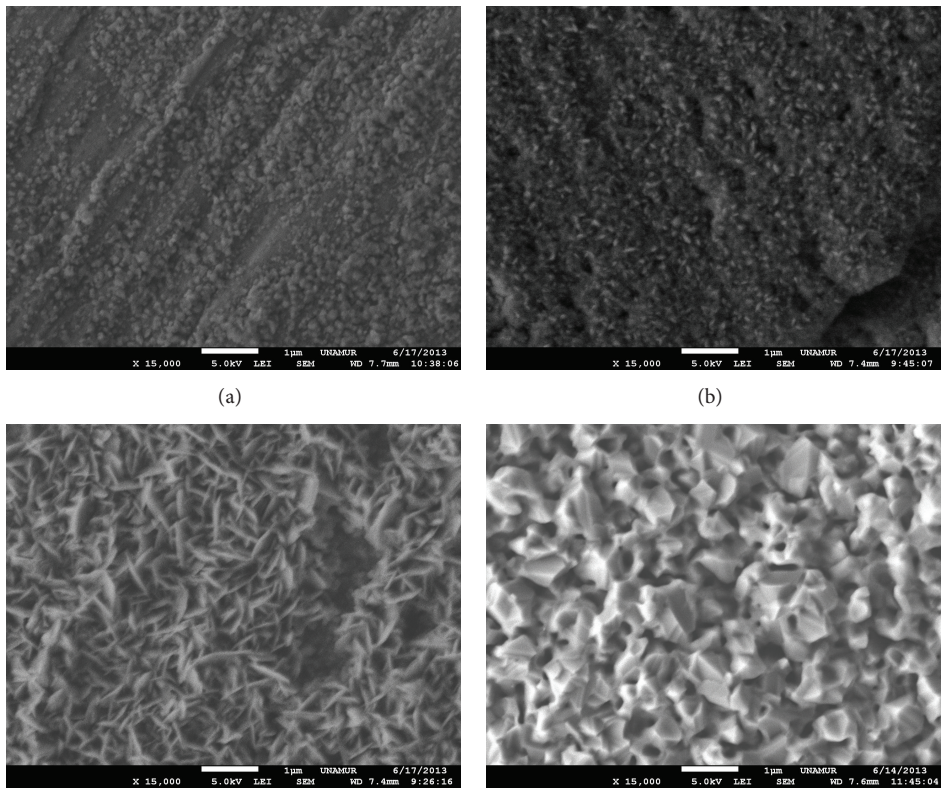

(a) (b) (c) (d)

Figure 2: Typical morphology of the surface scales of PM2000 after 7 h exposure at 873 K (a), 1073 K (b), 1173 K (c), and 1473 K (d).

Concerning the morphology of the oxide obtained at 1473 K, which can be seen in Figure 2(d), the formation of a bulk porous microstructure is observable, with a quite different microstructure in comparison with the a, b, c specimens. The Al_2O_3 (equiaxed grains) microstructure colonies develop into vermicular morphology containing larger scale interconnected porosity.

Data are analyzed in order to reveal the calcination effectiveness and to check the stoichiometry of the as-prepared oxide films; the results are reported in Table 1.

Figure 3(a) shows the EDX analysis samples of PM2000 (as-received and oxidized). The analyzed oxide layers are rich in Fe, Cr, and Al in the interval of temperatures between 873 K and 1073 K. For temperatures above 1173 K, Al_2O_3 becomes predominant. An example of EDX spectra of oxidized PM2000 at 1473 K is shown in Figure 3(b). As shown in Figure 3(b), the presence of Mg appears more important as the temperature increases in the α-Al_2O_3 layer. Its dissemination to the external interface is favored by higher temperatures [13].

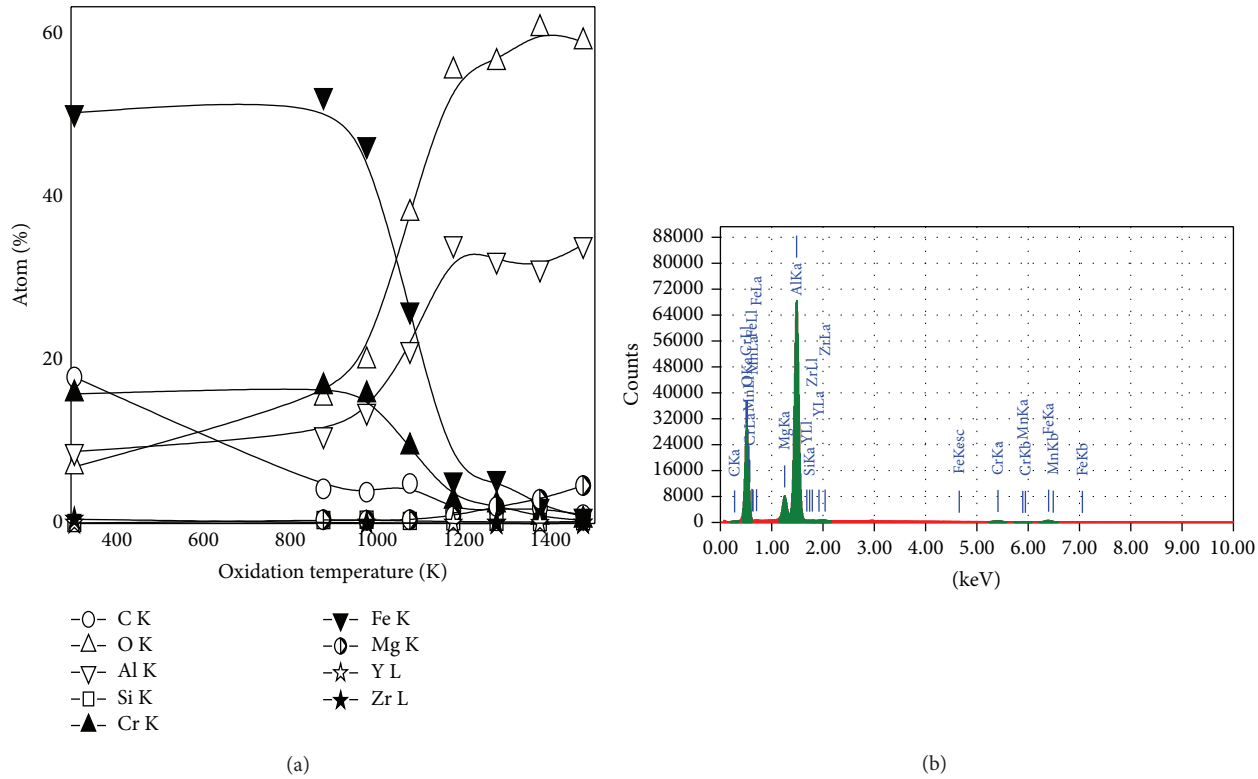

Figure 3: EDX analysis samples of as-received PM2000 and oxidized PM2000 (a) and example of EDX spectra of oxidized PM2000 at 1473 K used for composition calculation (b) (see Table 1).

2.4. XRD Results. PM2000 is iron-based (Fe-Cr-Al) with a ferritic matrix (α-Fe) as shown in Figure 4(a) and is mechanically alloyed with Y_2O_3 and ZrO_2 dispersion material. Before oxidation, at room temperature, native oxide, thin film exists on the alloy surface, with only several nanometers in thickness, and it consists of all the alloying elements as mentioned in literature [14]. This native oxides is Al_2O_3 and a mixture of oxides as Fe, and Cr. The oxide formation at elevated temperatures can be separated in three steps. First, at relatively low temperatures (873, 973, and 1073 K), a mixed oxide similar to the preexisting native oxide forms, the XRD does not allow the revelation of these oxides (they are revealed by SEM observations and detected by FTIR, EDX, and XPS analysis). Second, at 1173 K, the XRD pattern obtained reveals, in Figure 4(b), the presence of the α-Fe, α-Al_2O_3, transition Al_2O_3, and different phases of oxides: Fe_2O_3 or $(Fe_{0.6}Cr_{0.4})_2O_3$ or Cr_2O_3. Third, at higher temperature greater than 1373 K, the main existing oxide is α-Al_2O_3 (Figure 4(c)).

Information on the crystallite size (D) for the compounds (i.e., α-Al_2O_3) was obtained from the full width at half maximum of the diffraction peaks using the Scherrer formula [15]:

$$D = \frac{0.94\lambda}{\beta\,(hkl)\cos\theta\,(hkl)}, \quad (1)$$

where λ, $\theta(hkl)$, and $\beta(hkl)$ are the X-ray wavelength (0.15418 nm), Bragg diffraction angle, and line width at half maximum, respectively. The values of the $\beta(hkl)$ and $\theta(hkl)$ parameters from the XRD peak are estimated by Gaussian fitting. This formula is not limited by the preferential orientation and is valid for an ordinary XRD profile. To improve the statistics, the most intense peaks in the profiles were chosen to determine the crystallite size. The results are reported in Table 2.

Table 2: Crystallite sizes versus oxidation temperature.

Oxidation temperature	1273 K	1373 K	1473 K
Crystallite size D (nm)	36 ± 8	40 ± 8	44 ± 8

2.5. FTIR Characterizations of the Transition Al_2O_3 on Oxidized PM2000 Alloys. The FTIR spectral signatures of both α-Al_2O_3 and metastable forms have been thoroughly addressed in the literature using both experimental and theoretical simulations [16–19]. It is now possible to detect the presence of transition Al_2O_3 and perhaps their nature on oxide scales formed by oxidation of alumino-former alloys. For this purpose, PM2000 samples (PM2000, ODS alloy), oxidized at different temperatures (from 873 K to 1473 K in air for 7 hours) were studied by IR spectroscopy. FTIR spectra are reported in Figure 5. The spectrum (Figure 6(a)) at 873 K in the range 400–1000 cm^{-1} represents a poorly crystallized structure characterized by a broadband with no apparent thin peak. This signature is that of the γ-Al_2O_3 (the broad

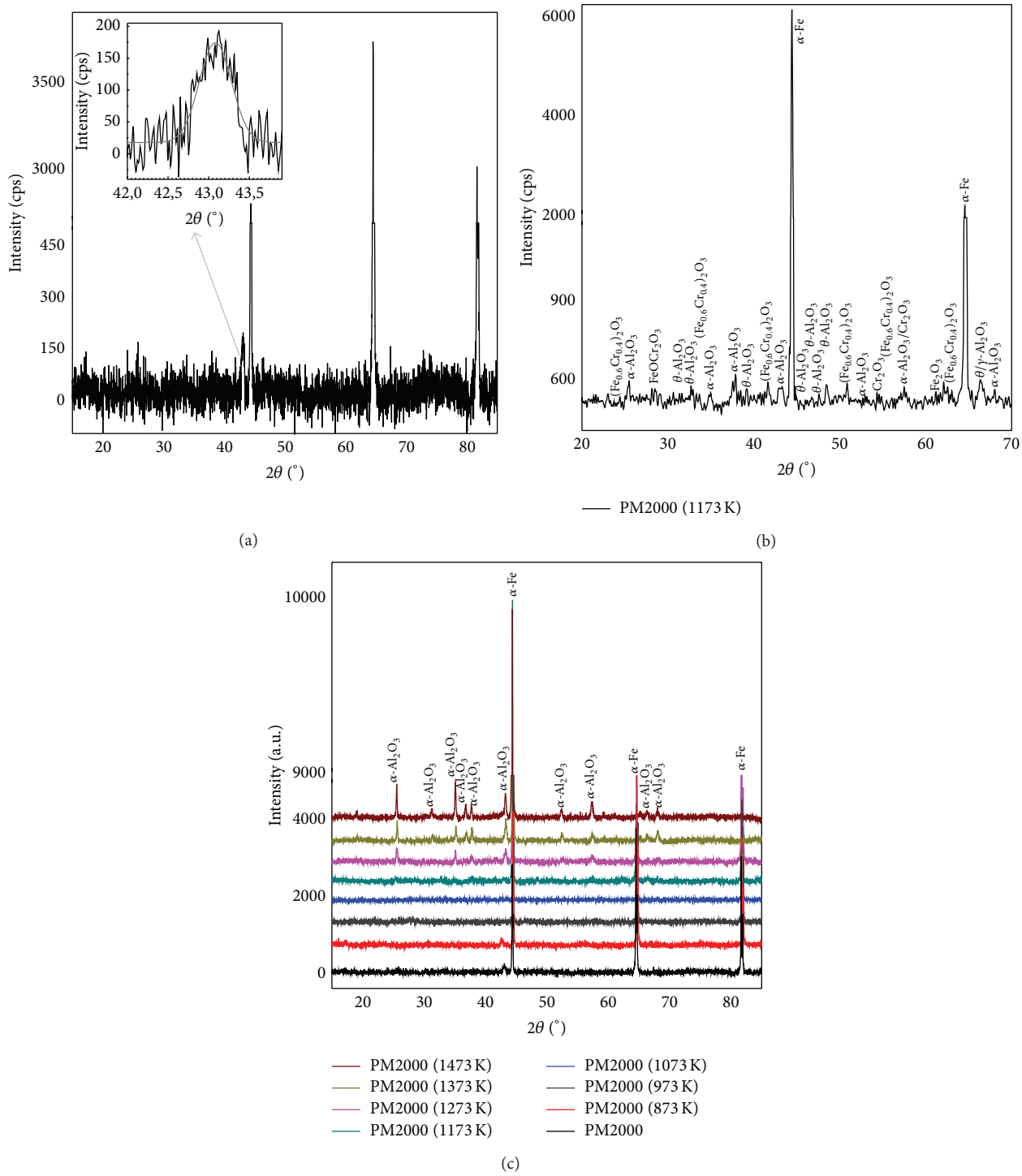

Figure 4: XRD powder patterns of as-received PM2000 (a), heat treated on air at 1173 K (b), and heat treated on air from 873 to 1473 K (c).

extending band in the range 400–700 cm^{-1} indicates the existence of amorphous structure or disordered defects). The FTIR spectrum obtained after oxidation in air for 7 h of a PM2000 sample at 1073 K (Figure 6(b)) differs from the previous one. Peaks appear, indicating the presence of a better crystallized phase; the presence of α-Al_2O_3 is also detected in this spectrum. The main peaks at 459, 595, and 656 cm^{-1} can be assigned to the Al–O stretching mode in octahedral structure; bands around 715 cm^{-1} and 1072 cm^{-1} are related to Al–O stretching mode in tetrahedron and symmetric bending of Al–O–H, respectively. The broad absorbance bands between 900 and 1100 cm^{-1} are assigned to O–H deformation vibrations. Thus, the transformation from the amorphous state to α-Al_2O_3 can be identified from the appearance of 720

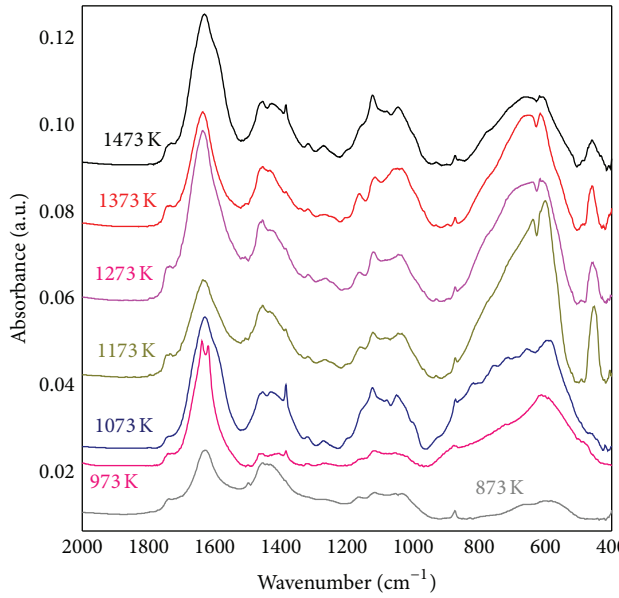

Figure 5: FTIR spectra of oxidized PM2000 at various temperatures from 873 K to 1473 K.

and 1072 cm^{-1} bands, due to the differences in the sites of Al cations and the distribution of H in these oxides [20–22]. The presence of Fe oxides or Fe-Al oxide mixtures can make this spectrum more complex. The outer surface of the Al_2O_3 scale formed on PM2000 after 7 h oxidation at 1073 K in air was observed by SEM (Figure 2). The Al_2O_3 morphology is a characteristic of transition Al_2O_3. However, we cannot say whether it is δ or θ (or even mixtures) that are present at this temperature. The spectra (Figures 6(c) and 6(d)) of the oxidized alloys 1173, 1273, 1373, and 1473 K indicate clearly the presence of α-Al_2O_3. Thus, the IR spectroscopy in the range 400–1000 cm^{-1} can be used as a fast and easy tool to distinguish the presence of transition Al_2O_3 phases on oxidized high temperature materials and to determine whether γ, δ, or θ-Al_2O_3 are present. The α-Al_2O_3 is clearly identified by its spectra shown in Figures 6(c) and 6(d). This allowed to clearly differentiate the transition Al_2O_3 from the α-Al_2O_3 and, amongst the transition Al_2O_3, to differentiate the characteristic IR spectrum of γ-δ phases from that of the θ phase [20, 21]. Peak observed at ~873 cm^{-1} is due to out-of-plane bending vibration (υ4–CO_3^{2-}) of carbonate.

2.6. XPS Results. XPS is sensitive to the chemical composition and the local environment of atoms in the crystal structure, which is reflected by the changes in the binding energy and the occurrence of multiple bands associated with different chemical environments. In the literature, the XPS analyses of Al, Fe, Cr, Mg, and Si oxides were performed and interpreted for the O1s, Al2p, Fe2p, Cr2p, Mg1s, Si1s, and C1s. XPS bands data were compared with the values reported in the literature [23–29]. XPS spectra of native oxides Fe-Cr oxides, transition Al_2O_3, and α-Al_2O_3 have been studied by spectral characterization of each sample (the as-received PM2000, and after oxidation from 873 to 1473 K). Figure 7 shows the XPS survey spectra and the spectrum of each sample reveals the peaks for O1s, Al2p, Fe2p, Cr2p, Mg1s, Si2p, and C1s, which indicates the presence of O, Al, Fe, Cr, Mg, Si, and C.

The XPS Al2p spectra for treated and as-received PM2000 are shown in Figures 8(a) and 8(b) and Figures 9(a), 9(b), and 9(c). The Al2p spectra are shifted 1 eV to higher binding energy (E_b) in the order α-Al_2O_3 < θ-Al_2O_3 < γ-Al_2O_3. A double band is observed for the as-received PM2000; the first is located at 74.83 eV (FWHM 1.90 eV) corresponding to Al-O state and the second is located at 72.30 eV (FWHM 3.36 eV) corresponding to Al-M state. The Al2p band of oxidized alloy at 873 K (Figure 8(a)) shows a single peak located at 75.06 eV (FWMH 2.22 eV), which corresponds to the γ-Al_2O_3 form (as analyzed by FTIR spectroscopy). At 1273 K, the peak at 74.25 eV (FWMH: 1.67 eV) is affected to α-Al_2O_3 and the peak at 74.82 eV (FWMH 2.56 eV) is affected to θ-Al_2O_3 (Figure 8(b)). The results obtained for the valence Al2p for these alloys show that the variations in binding energies are within an interval of about 1 eV; these are in good agreement with previous observations [23, 26, 27]. The evolution of α-Al_2O_3 Al2p peaks is represented in Figures 9(a) and 9(b), for temperature increasing from 873 to 1473 K. At 1373 K, the α-Al_2O_3 peak is symmetrical and the BE position is given at 74.45 eV (FWHM 1.97 eV). The XPS decomposition peaks (Figure 9(b)) related to the energies Al2p bands are used to estimate the evolution percentage of the thermal α-Al_2O_3 phase between 873 and 1473 K (Figure 9(c)). This trend can be divided into three parts. First, at temperatures between 873 and 1073 K, the percentage is low and does not exceed 15%; this part corresponds to the γ-Al_2O_3 and the (Fe, Cr) oxides formation. The second portion is between 1073 and 1173/1273 K; the percentage of Al is growing rapidly and has a high slope, which means a significant growth of thermal α-Al_2O_3 and θ-Al_2O_3 in this field. Finally, in a step between 1173/1273 and 1473 K, α-Al_2O_3 takes place.

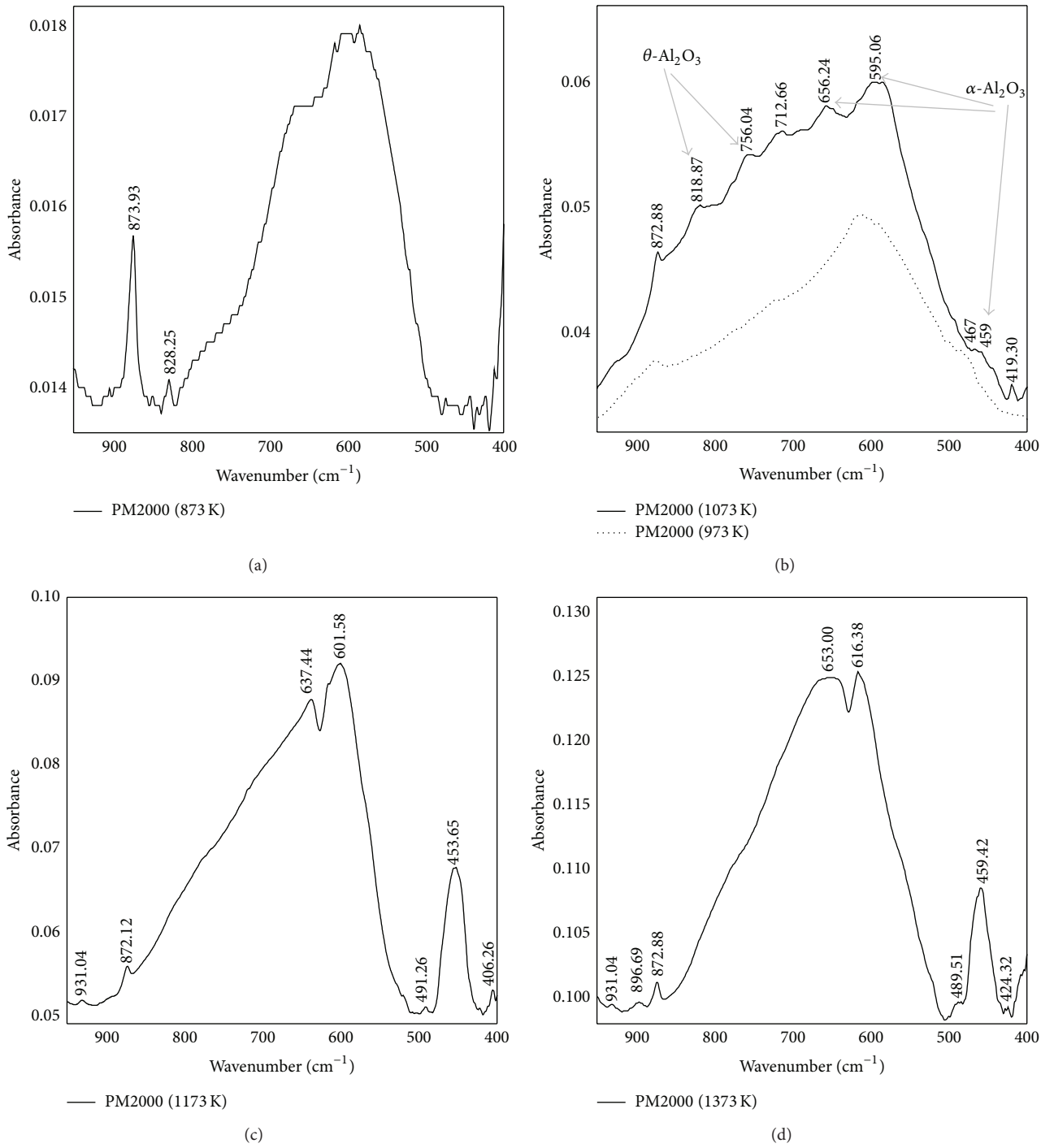

Figure 6: FTIR spectra of oxidized PM2000 at 873 K (a), 973 K and 1073 K (b), 1173 K (c), and 1373 K (d).

The O1s peaks are less symmetrical (relative to Al2p peaks), more complex, and more sensitive to the different states of the minerals. In fact, the O1s band is very important due to its intensity, which allows it to be more sensitive and hence more exploitable, according to the literature [23–26]. This band can be decomposed into multiple parts: the O1s band corresponding to (Fe, Cr) oxides is located at ~529 eV, the O1s band corresponding to Al_2O_3 oxides is located at ~531 eV, the O1s band corresponding to the OH groups is located at ~532 eV, and the O1s band indicating the presence of amorphous mixtures containing H_2O is located at ~533.5 eV.

Figure 10(a) represents O1s peaks of as-received and treated PM2000. We note that these peaks exhibit significant differences depending on the compound state. In the as-received PM2000, the energy of O1s is shifted to 531.84 eV

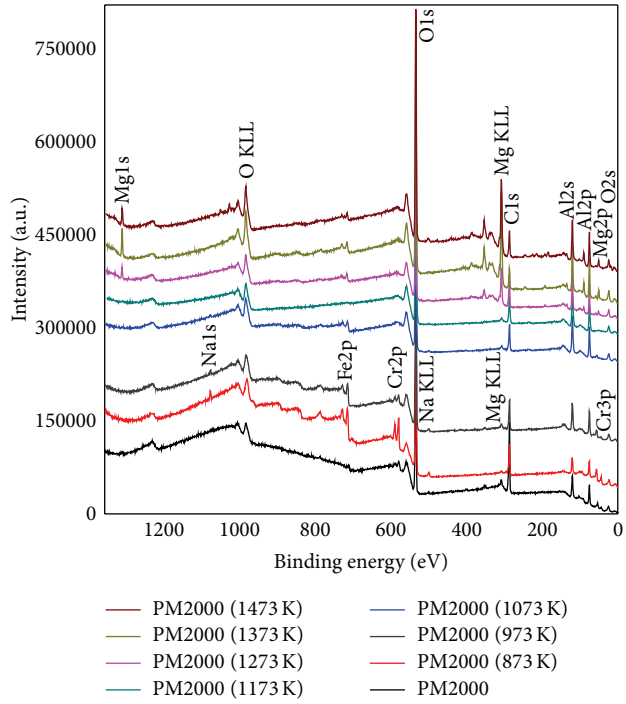

Figure 7: XPS survey spectra of as-received and oxidized PM2000.

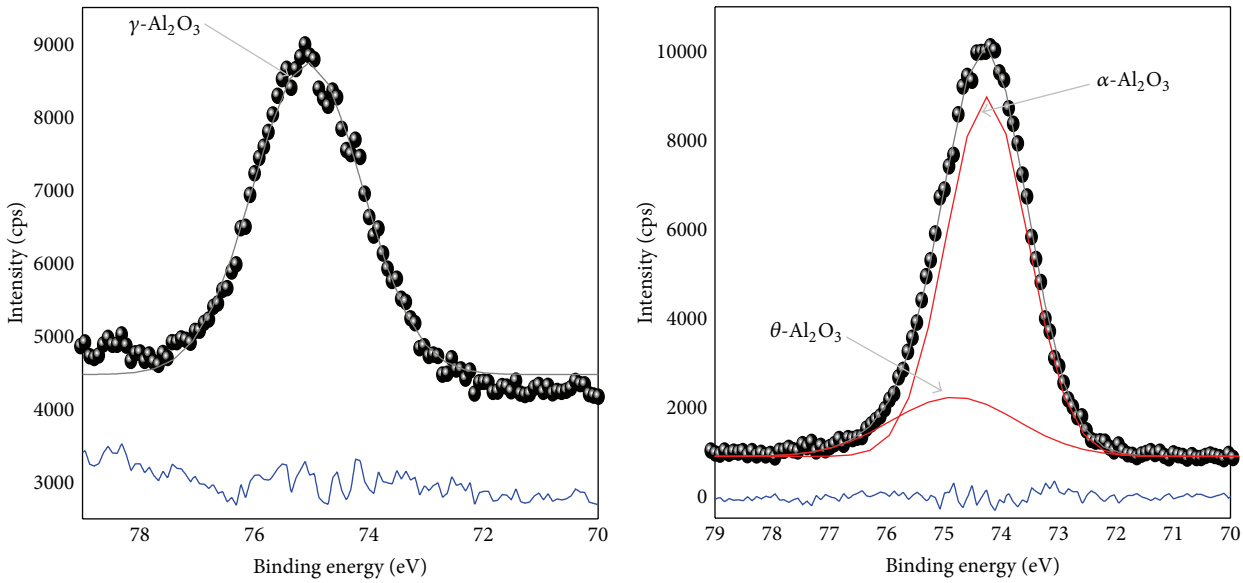

PM2000 (873 K)

Gaussian fit peak	BE (eV)	FWHM (eV)	Atom (%)
Al2p	75.06	2.22	100

(a)

PM2000 (1273 K)

Gaussian fit peak	BE (eV)	FWHM (eV)	Atom (%)
Al2p	74.25	1.68	79.86
Al2p	74.82	2.56	20.14

(b)

Figure 8: Single Al2p peak of oxidized PM2000 at 873 K (a) and decomposed Al2p peak of oxidized PM2000 at 1273 K (b).

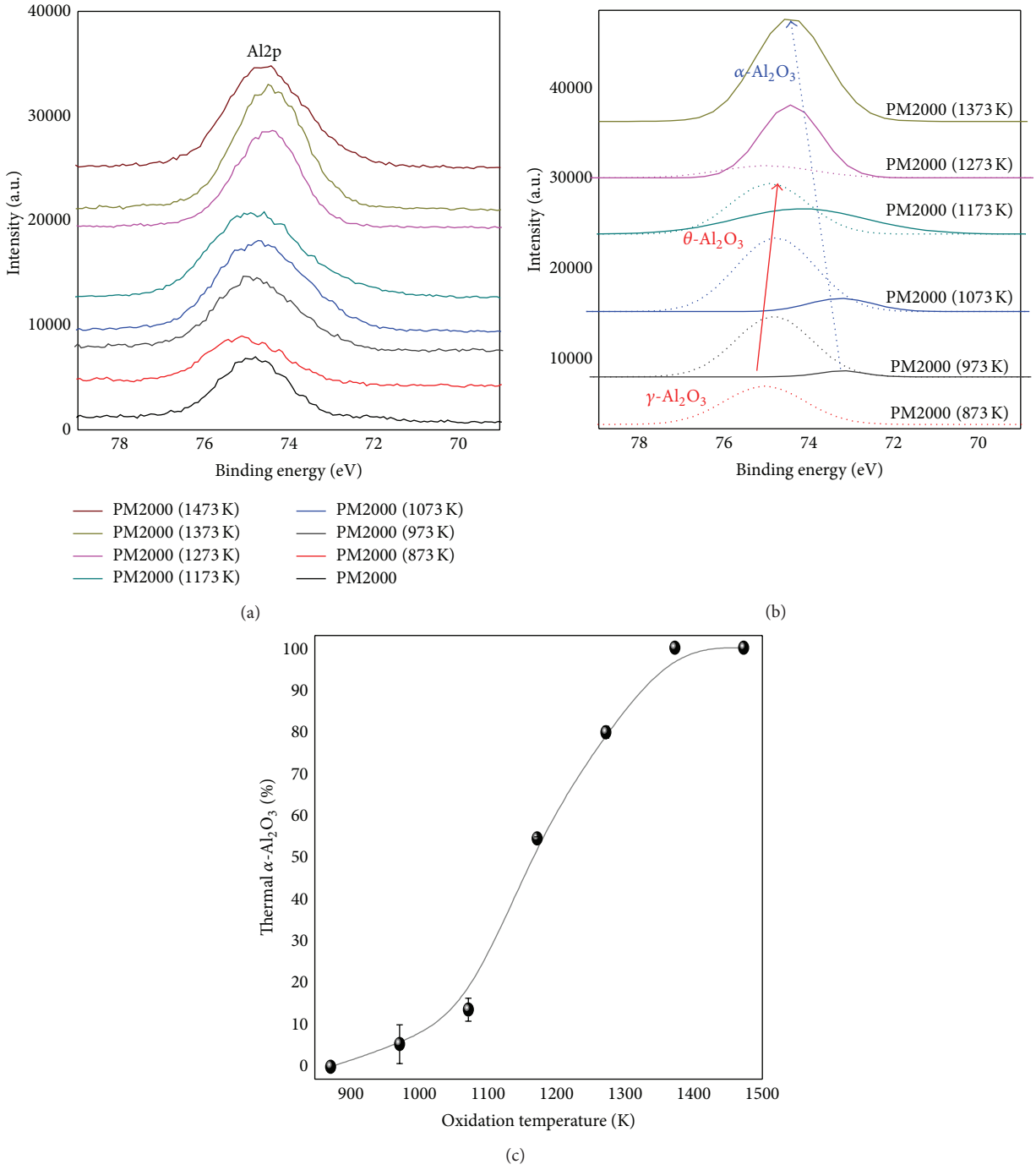

FIGURE 9: Al2p XPS spectra of the treated and as-received PM2000 (a) and Al2p XPS decomposed spectra of PM2000 (b) evolution percentage of the thermal α-Al_2O_3 phase between 873 and 1473 K (c).

(FWHM 2.54 eV), the surface of the material contains a few thin native oxide. These native oxides are mainly composed of Al, Fe, and Cr. The O1s core level photoemission spectra for PM2000 (873) and PM2000 (973) confirm the presence of, at least, two oxides and eventually hydroxides. At 873 K (Figure 10(b)), when decomposed, the peak at 529.69 eV (FWHM 1.28 eV) indicates the presence of the Fe, Cr oxides [28, 29], the peak at 531.67 eV (FWHM 2.11 eV) indicates the presence of the transition Al_2O_3 oxides (the γ-Al_2O_3 form), and the O1s band indicating the presence hydroxyls is located at 532.80 eV (FWHM 1.50 eV). The peak at 1073 K (Figure 10(c)), when decomposed, indicates the presence of the transition Al_2O_3 located at 531.43 eV (FWHM 2.83 eV) with the percentage of ~94.3%, and the peak at 529 eV (FWHM 1.91 eV) indicates the presence of (Fe, Cr) oxide with the percentage of ~5.7%. For PM2000 (1373) shown

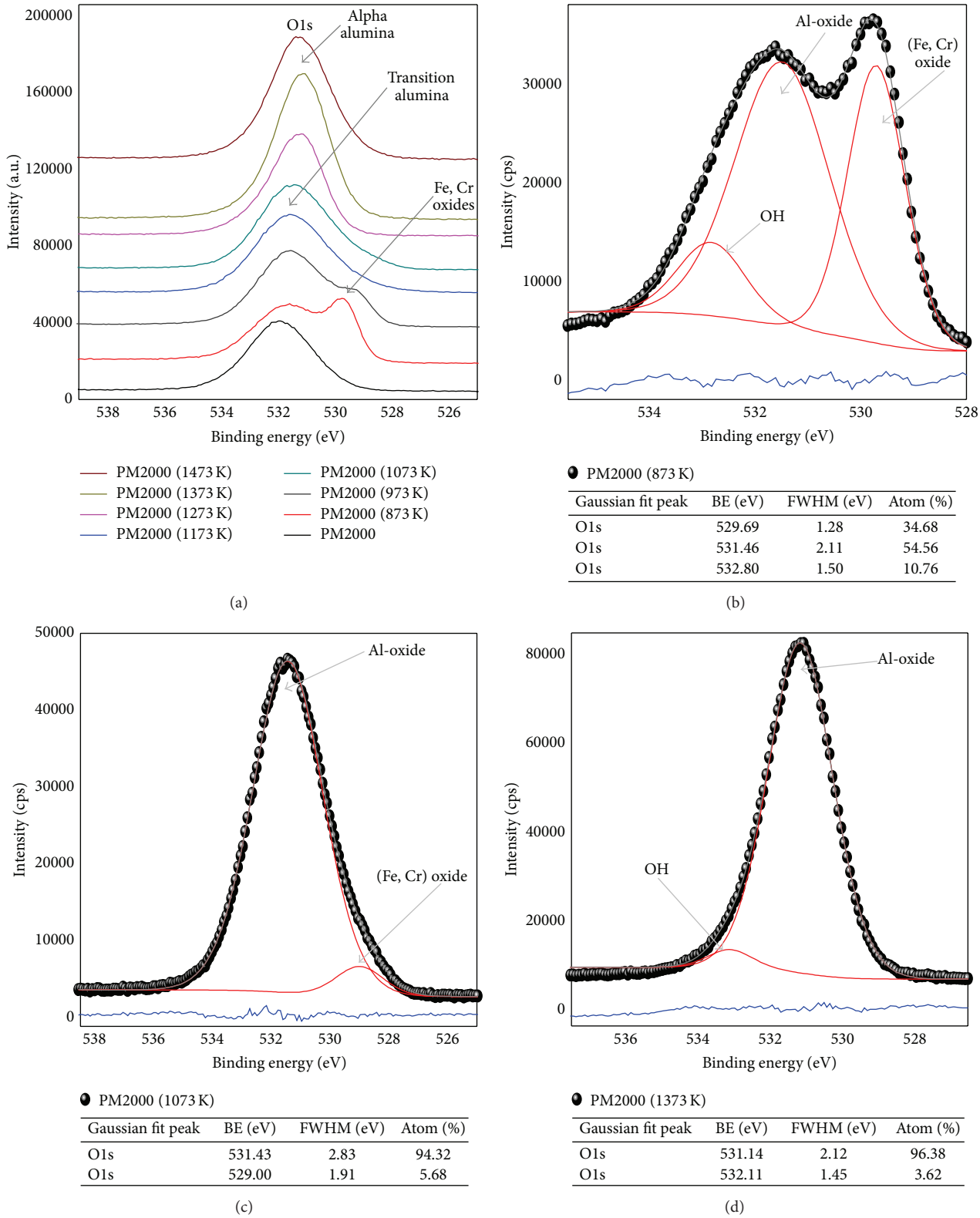

Gaussian fit peak	BE (eV)	FWHM (eV)	Atom (%)
O1s	529.69	1.28	34.68
O1s	531.46	2.11	54.56
O1s	532.80	1.50	10.76

Gaussian fit peak	BE (eV)	FWHM (eV)	Atom (%)
O1s	531.43	2.83	94.32
O1s	529.00	1.91	5.68

Gaussian fit peak	BE (eV)	FWHM (eV)	Atom (%)
O1s	531.14	2.12	96.38
O1s	532.11	1.45	3.62

Figure 10: XPS spectra in the O1s region for as-received and treated PM2000 at various temperatures (a), decomposed O1s peaks of oxidized PM2000 at 873 K (b), decomposed O1s peaks of oxidized PM2000 at 1073 K (c), and decomposed O1s peaks of oxidized PM2000 at 1373 K (d).

in Figure 10(d), the wide peak at 531.14 (FWHM 2.12 eV) indicates the presence of the α-Al_2O_3 with the percentage of ~96%, and a small peak at 532.11 eV (1.45 eV) due to the presence of the OH groups.

The Fe oxidation state of the oxides formed at various temperatures oxidations can be derived from the Fe2p spectra in Figure 11. $Fe2p_{3/2}$ and $Fe2p_{1/2}$ main line peak positions are 710.5 and 724.0 eV, respectively, which is in excellent agreement with the literature values for the mixed Fe_2O_3-(maghemite-) Fe_3O_4 (magnetite) surface [30–32]. In addition, the occurrence and intensity of the so-called $Fe2p_{3/2}$ charge-transfer satellites, which appear additionally to the $Fe2p_{3/2}$ main line, indicate the oxidation state of different Fe oxides. In the case of Fe_2O_3, the Fe^{3+} charge-transfer satellite should occur at 719 eV, while for divalent FeO, the Fe^{2+} satellite appears at 715.5 eV. For the mixed valence state of Fe_3O_4 ($Fe^{3+}:Fe^{2+} = 2:1$), both satellites add up in such a way that the spectral region between the $2p_{3/2}$ and $2p_{1/2}$ main lines becomes smooth and less structured [28–33]. In all samples, Fe2p peaks have asymmetric shape. In the spectrum of the as-received PM2000, the peaks corresponding to metallic Fe are specified at 706.93 eV and 707.89 eV, satellite is given at 720.16 eV, and the $Fe2p_{3/2}$ peak of native oxides is located at 711.33 eV. When oxidized at 873 K and 973 K, the spectra corresponding to the $Fe2p_{3/2}$ and $Fe2p_{1/2}$ bands are rather wider; peaks shifted at ~711 eV and 724 eV, respectively. The satellite at 719.22 eV is well defined. At 1200°C, the peaks $Fe2p_{3/2}$ and $Fe2p_{1/2}$ are given to the binding energies near ~714 eV and ~725 eV. The decomposition of the spectrum between 716 and 725 eV can give satellites at 720 eV; these peaks indicate the presence of α-Fe_2O_3.

The Cr oxidation state of the oxides formed at various temperatures oxidations can be derived from the Cr2p spectra in Figure 12, and the peaks observed at 577 eV and 586.5 eV indicate $Cr2p_{3/2}$ electrons and Cr_2O_3 presence in the formed oxide. A satellite of the $Cr2p_{3/2}$ peak overlaps the $Cr2p_{1/2}$ component in Cr_2O_3. The peaks at 577.6 eV and 586.38 suggest $Cr2p_{3/2}$ and $Cr2p_{1/2}$ core electrons, respectively. The $Cr2p_{3/2}$ and $2p_{1/2}$ main line peak positions are in the range 775–582 eV and 582–590 eV, respectively, being in excellent agreement with literature values [34, 35]. In all samples, Cr2p peaks have asymmetric shape. In the spectrum of the as-received PM2000, the peaks corresponding to metallic Cr at 574.39 eV and 575.02 eV are identified. A $Cr2p_{3/2}$ peak of native oxides is located in the range 576–579 eV. When oxidizing at 873 K and 973 K, the spectra corresponding to the $Cr2p_{3/2}$ and $Cr2p_{1/2}$ bands are significant and located in the range 576–580 eV and 584–590 eV, respectively (Figures 12(a) and 12(b)). The existence of Cr_2O_3 was IR from a peak at 579.60 eV. For the oxidations at temperatures above 1073 K, these bands become negligible.

The SiO_2 and SiC are found by XPS peak (Si2p bands) positions 99.4 eV, 103.5 eV, and 100.3 eV, respectively. Peaks obtained are 100.87 eV and 97.75 eV (Figure 13), which reveals the presence of SiC and eventually Si. This compound is quite stable, since the alloy receiver (native oxide) and the amount do not change during oxidation. The addition of small quantities of colloidal SiO_2 to a commercial Al_2O_3 powder has a significant effect on its densification and microstructure evolution [36, 37]. SiO_2 has a detrimental effect on the Al_2O_3 densification behavior particularly during the intermediate stage of sintering (from 1473 to 1673 K).

As mentioned above, the presence of Mg appears more important as the temperature increases. Its dissemination to the external interface is favored by higher temperatures as shown in Figure 14. Mg doping α-Al_2O_3 improved densification and elimination of residual porosity [38]. Works demonstrate that Mg additions uniformly distributed over a nanometer-sized Al_2O_3 powder have no effect on the γ to δ phase transition, raise the densification rate in the rapid-sintering stage, and increase the net shrinkage [39].

2.7. Adventitious C (Carbon). The decomposition of the C1s signal in the domain (oxidation PM2000 at 873–1473 K) results in too bands (Figures 15(a) and 15(b)). The peak at ~285.0 eV is associated with the binding energy of the C atoms in aromatic C–C/C–H [40], and the peak at 288.55 eV can be attributed to the binding energy of the carboxylic group (O–C=O), which is in agreement with the literature results [41].

3. Conclusion

The aim of this work was to determine whether IR spectroscopy and XPS could allow us to easily distinguish the different structural varieties of Al_2O_3 and therefore be used as a rapid diagnostics to evidence the phases present in the protective layers of high temperature materials. It was thus possible to determine the FTIR spectra of Al_2O_3 phases and the XPS analysis at different temperatures of oxidation and to evidence a continuous evolution leading to the simultaneous presence of several Al_2O_3 phases. These results have allowed us to determine some characteristic IR and XPS peaks, that is, signatures, for the various transition Al_2O_3 phases and α-Al_2O_3. Using these IR and XPS signatures, it is possible to detect the presence of transition Al_2O_3 naturally grown on Al_2O_3-former alloys. A detailed example is presented for the oxidation of PM2000 ODS alloy. Indeed, many high temperature metallic materials develop Al_2O_3 scales that can act as protective layer against an aggressive environment. In the first stage, mixed Fe, Cr oxides, and transition Al_2O_3 appear; afterwards Al_2O_3 oxides become gradually the majority as the oxidation temperature increases before transformation into the most stable α-Al_2O_3 structure. Although the physical properties of the transition Al_2O_3 differ, their identification is not straightforward.

Highlights

(i) FTIR and XPS techniques were used to clarify the evolution of oxides formed on the alloy PM2000.

(ii) The percentage of the thermal α-Al_2O_3 formation was estimated by XPS analysis as a function of temperature.

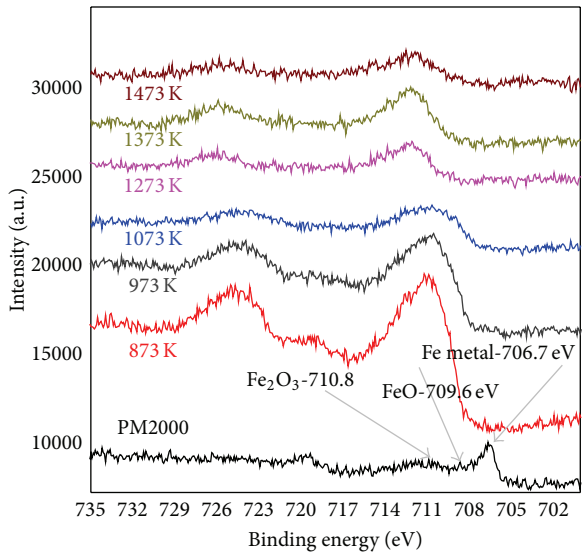

(a)

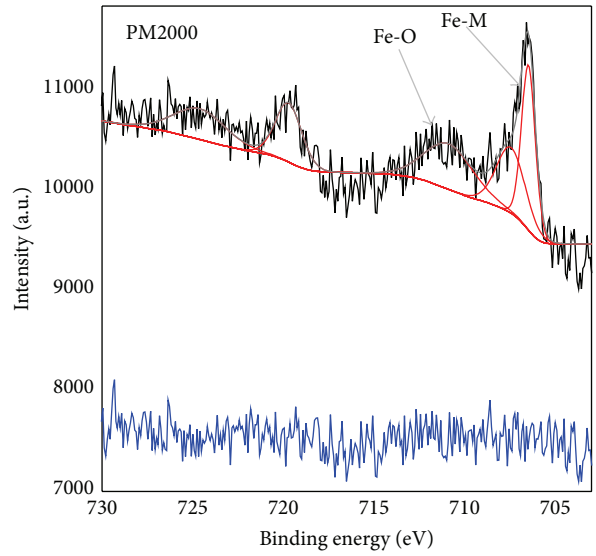

PM2000 (1473 K)

Gaussian fit peak	BE (eV)	FWHM (eV)	Atom (%)
$Fe2p_{3/2}$	706.48	0.89	23.68
$Fe2p_{3/2}$	707.44	1.88	19.86
$Fe2p_{3/2}$	710.88	3.14	23.13
$Fe2p_{3/2}$	719.71	1.71	16.44
$Fe2p_{1/2}$	724.62	3.37	16.88

(b)

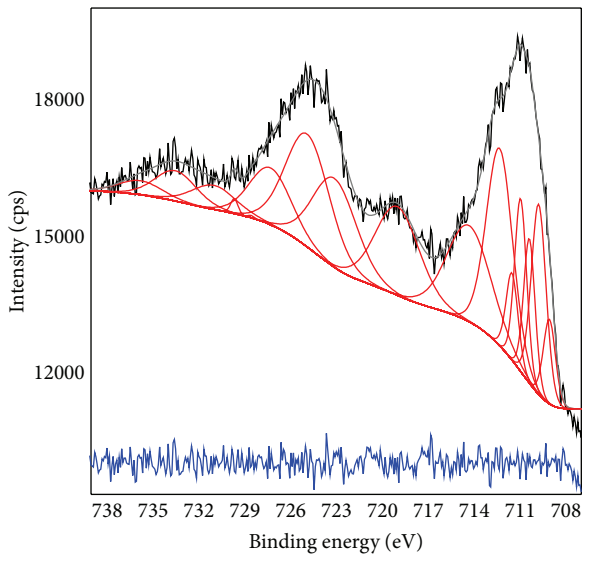

PM2000 (873 K)

(c)

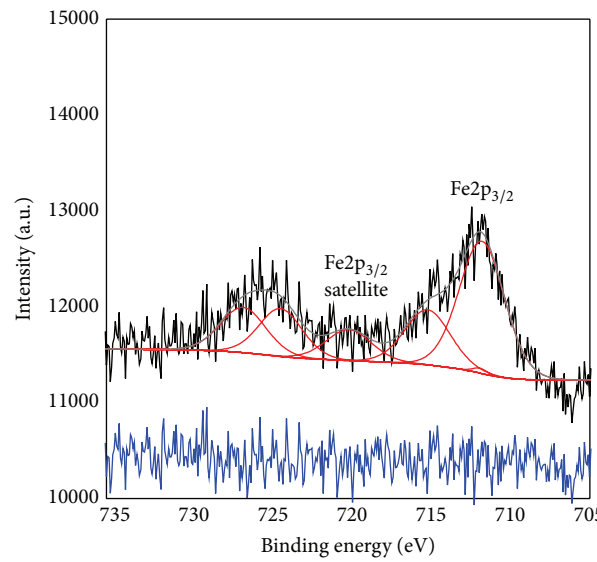

PM2000 (1473 K)

Gaussian fit peak	BE (eV)	FWHM (eV)	Atom (%)
$Fe2p_{3/2}$	711.81	3.36	42.44
$Fe2p_{3/2}$	711.93	1.07	00.50
$Fe2p_{3/2}$	715.23	3.37	17.70
$Fe2p_{3/2}$	720.20	3.36	09.96
$Fe2p_{1/2}$	724.51	3.20	14.74
$Fe2p_{1/2}$	726.87	3.37	14.74

(d)

Figure 11: XPS spectra in the Fe2p region for as-received and treated PM2000 at various temperatures (a), decomposed O1s peaks of as-received PM2000 (b), decomposed O1s peaks of oxidized PM2000 at 873 K (c), and decomposed O1s peaks of oxidized PM2000 at 1473 K (d).

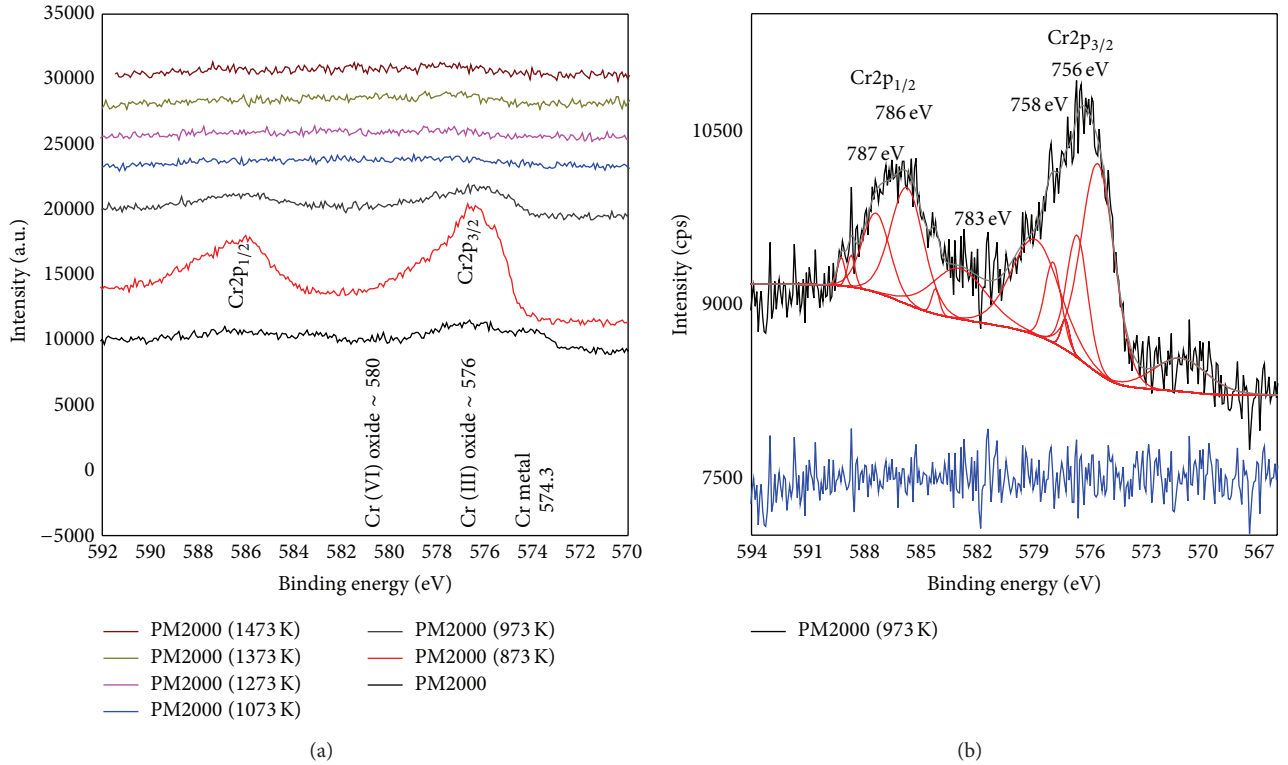

FIGURE 12: XPS spectra in the Cr2p region for as-received and treated PM2000 at various temperatures (a) and decomposed Cr2p peaks of oxidized PM2000 at 973 K (b).

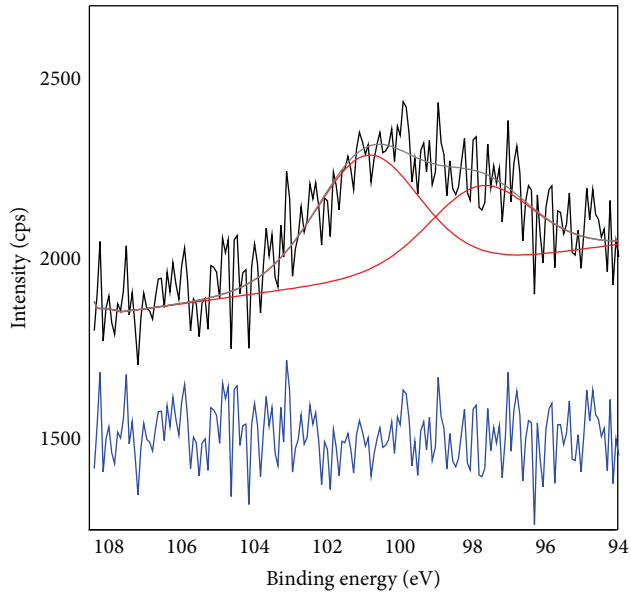

Gaussian fit peak	BE (eV)	FWHM (eV)	Atom (%)
Si2p	97.75	3.95	38.42
Si2p	100.87	3.95	61.58

FIGURE 13: Decomposed Si2p peaks of oxidized PM2000 at 1073 K.

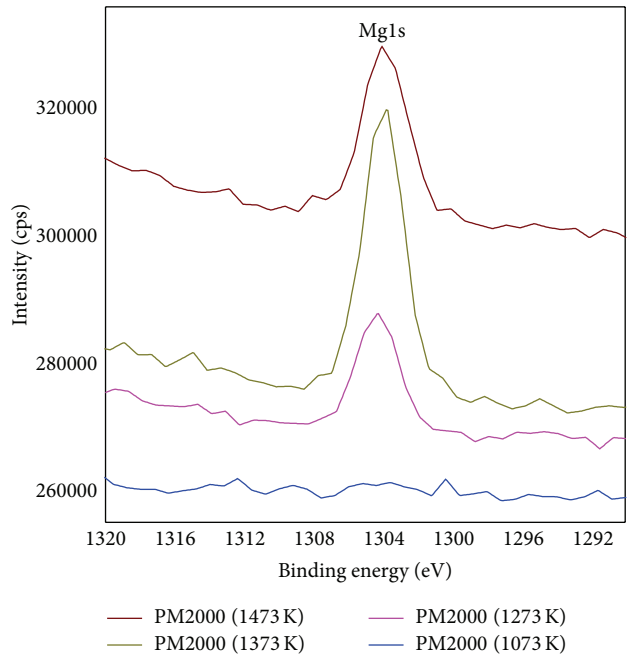

Figure 14: XPS spectra in the Mg2p region for treated PM2000 from 1073 K to 1473 K.

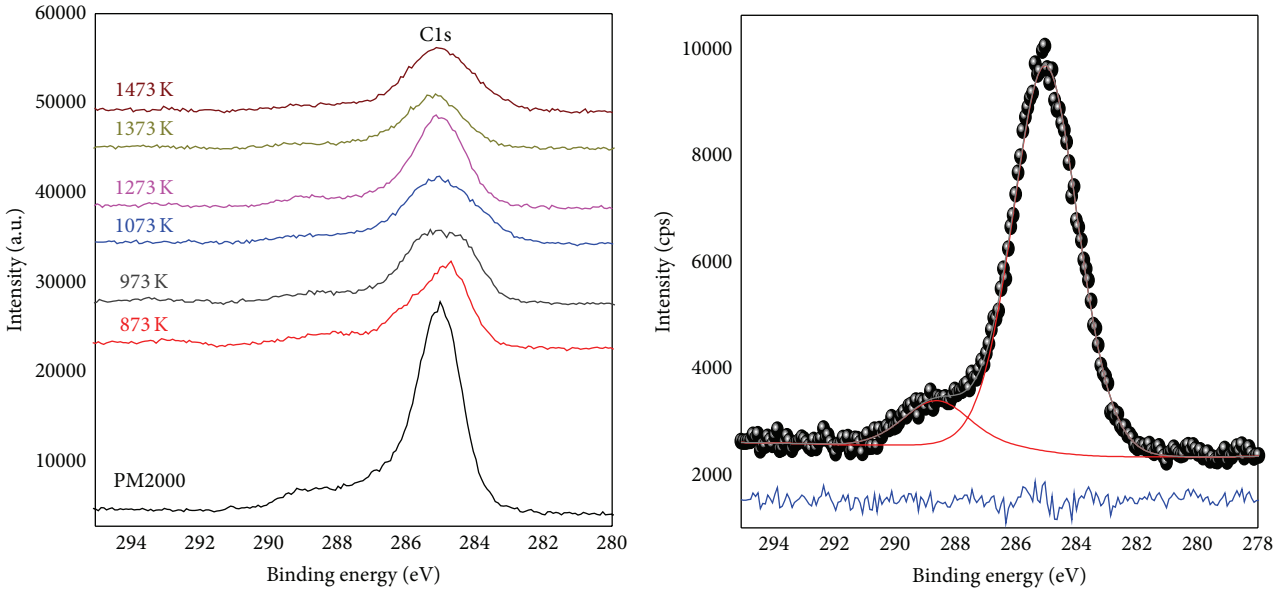

Gaussian fit peak	BE (eV)	FWHM (eV)	Atom (%)
C1s	284.98	2.95	89.40
C1s	288.56	3.00	10.60

(a) (b)

Figure 15: XPS spectra in the C1s region for treated and as-received PM2000 at various temperatures (a) and decomposed C1s peak of oxidized PM2000 at 1073 K (b).

Conflict of Interests

The authors declare that there is no conflict of interests regarding the publication of this paper.

Acknowledgments

This work was partly supported by the National Project Research (PNR) and LASPI^{2}A laboratory of Khenchela University, Algeria.

References

[1] R. Molins and A. M. Huntz, "Recent improvements in the understanding of alumina film formation and durability," *Materials Science Forum*, vol. 461–464, no. I, pp. 29–36, 2004.

[2] S. Chevalier, R. Molins, O. Heintz, and J. P. Larpin, "Which tool to distinguish transient alumina from alpha alumina in thermally grown alumina scales?" *Materials at High Temperatures*, vol. 22, no. 3-4, pp. 527–534, 2005.

[3] H. El Kadiri, R. Molins, Y. Bienvenu, and M. F. Horstemeyer, "Abnormal high growth rates of metastable Al_2O_3 on FeCrAl alloys," *Oxidation of Metals*, vol. 64, pp. 63–97, 2005.

[4] A. M. Huntz, P. Y. Hou, and R. Molins, "Study by deflection of the oxygen pressure influence on the phase transformation in Al_2O_3 thin films formed by oxidation of Fe_3Al," *Materials Science and Engineering A*, vol. 467, no. 1-2, pp. 59–70, 2007.

[5] L. Maréchal, B. Lesage, A. M. Huntz, and R. Molins, "Oxidation behavior of ODS Fe-Cr-Al alloys: aluminum depletion and lifetime," *Oxidation of Metals*, vol. 60, no. 1-2, pp. 1–28, 2003.

[6] M. H. Heinonen, K. Kokko, M. P. J. Punkkinen, E. Nurmi, J. Kollár, and L. Vitos, "Initial oxidation of Fe–Al and Fe–Cr–Al alloys: Cr as an Al_2O_3 Booster," *Oxidation of Metals*, vol. 76, no. 3-4, pp. 331–346, 2011.

[7] A. H. Heuer, T. Nakagawa, M. Z. Azar et al., "On the growth of Al_2O_3 scales," *Acta Materialia*, vol. 61, no. 18, pp. 6670–6683, 2013.

[8] M. F. López, A. Gutiéerrez, M. C. García-Alonso, and M. L. Escudero, "Surface analysis of a heat-treated, Al-containing, Fe-based superalloy," *Journal of Materials Research*, vol. 13, no. 12, pp. 3411–3416, 1998.

[9] J. Engkvist, U. Bexell, T. M. Grehk, and M. Olsson, "ToF-SIMS depth profiling of alumina scales formed on a FeCrAl high-temperature alloy," *Applied Surface Science*, vol. 231-232, pp. 850–853, 2004.

[10] F. A. Golightly, G. C. Wood, and F. H. Stott, "The early stages of development of α-Al_2O_3 scales on Fe-Cr-Al and Fe-Cr-Al-Y Alloys at high temperature," *Oxidation of Metals*, vol. 14, no. 3, pp. 217–234, 1980.

[11] D. Naumenko, W. J. Quadakkers, A. Galerie, Y. Wouters, and S. Jourdain, "Parameters affecting transient oxide formation on FeCrAl based foil and fibre materials," *Materials at High Temperatures*, vol. 20, no. 3, pp. 287–293, 2003.

[12] W. J. Quadakkers, J. Nicholls, D. Naumenko, J. Wilber, and L. Singheiser, *Materials Aspects in Automotive Catalytic Converters MACC*, H. Bode, Ed., Wiley-VCH, Munchen, Germany, 2001.

[13] P. Burtin, J. P. Brunelle, M. Pijolat, and M. Soustelle, "Influence of surface area and additives on the thermal stability of transition Al_2O_3 catalyst supports. I: kinetic data," *Applied Catalysis*, vol. 34, pp. 225–238, 1987.

[14] P. Y. Hou, X. F. Zhang, and R. M. Cannon, "Impurity distribution in Al_2O_3 formed on an FeCrAl alloy," *Scripta Materialia*, vol. 50, no. 1, pp. 45–49, 2004.

[15] B. D. Cullity, *Elements of XRD*, Addison-Wesley, Reading, Mass, USA, 2nd edition, 1978.

[16] A. Boumaza, L. Favaro, J. Lédion et al., "Transition alumina phases induced by heat treatment of boehmite: an X-ray diffraction and infrared spectroscopy study," *Journal of Solid State Chemistry*, vol. 182, no. 5, pp. 1171–1176, 2009.

[17] L. Favaro, A. Boumaza, P. Roy et al., "Experimental and ab initio infrared study of χ-, κ- and α-aluminas formed from gibbsite," *Journal of Solid State Chemistry*, vol. 183, no. 4, pp. 901–908, 2010.

[18] R. Rinaldi and U. Schuchardt, "Factors responsible for the activity of Al_2O_3 surfaces in the catalytic epoxidation of cis-cyclooctene with aqueous H_2O_2," *Journal of Catalysis*, vol. 236, pp. 335–345, 2005.

[19] G. K. Priya, P. Padmaja, K. G. K. Warrier, A. D. Damodaran, and G. J. Aruldhas, "Dehydroxylation and high temperature phase formation in sol-gel boehmite characterized by Fourier transform infrared spectroscopy," *Journal of Materials Science Letters*, vol. 16, no. 19, pp. 1584–1587, 1997.

[20] W. W. Peng, P. Roy, L. Favaro et al., "Experimental and ab initio study of vibrational modes of stressed Al_2O_3 films formed by oxidation of Al alloys under different atmospheres," *Acta Materialia*, vol. 59, pp. 2723–2730, 2011.

[21] L. Shen, C. Hu, Y. Sakka, and Q. Huang, "Study of phase transformation behaviour of Al_2O_3 through precipitation method," *Journal of Physics D: Applied Physics*, vol. 45, no. 21, Article ID 215302, 2012.

[22] C. H. Shek, J. K. L. Lai, T. S. Gu, and G. M. Lin, "Transformation evolution and infrared absorption spectra of amorphous and crystalline nano-Al_2O_3 powders," *Nanostructured Materials*, vol. 8, no. 5, pp. 605–610, 1997.

[23] W. Fei, S. C. Kuiry, S. Seal, K. Scammon, N. Quick, and M. June, "High temperature surface oxidation of metallic fibres for hot gas filtration," *Surface Engineering*, vol. 18, no. 3, pp. 197–201, 2002.

[24] S. Chevalier, A. Galerie, O. Heintz, R. Chassagnon, and A. Crisci, "Thermal alumina scales on FeCrAl: characterization and growth mechanism," *Materials Science Forum*, vol. 595–598, pp. 915–922, 2008.

[25] G. Berthomé, E. N'Dah, Y. Wouters, and A. Galerie, "Temperature dependence of metastable alumina formation during thermal oxidation of FeCrAl foils," *Materials and Corrosion*, vol. 56, no. 6, pp. 389–392, 2005.

[26] J. T. Kloprogge, L. V. Duong, B. J. Wood, and R. L. Frost, "XPS study of the major minerals in bauxite: gibbsite, bayerite and (pseudo-)boehmite," *Journal of Colloid and Interface Science*, vol. 296, no. 2, pp. 572–576, 2006.

[27] H. E. Evans, W. M. Bowser, and W. H. Weinberg, "An XPS investigation of alumina thin films utilized in inelastic electron tunneling spectroscopy," *Applications of Surface Science*, vol. 5, no. 3, pp. 258–274, 1980.

[28] M. C. Biesinger, B. P. Payne, A. P. Grosvenor, L. W. M. Lau, A. R. Gerson, and R. S. C. Smart, "Resolving surface chemical states in XPS analysis of first row transition metals, oxides and hydroxides: Cr, Mn, Fe, Co and Ni," *Applied Surface Science*, vol. 257, no. 7, pp. 2717–2730, 2011.

[29] E. Paparazzo, "XPS and auger spectroscopy studies on mixtures of the oxides SiO_2, Al_2O_3, Fe_2O_3 and Cr_2O_3," *Journal of Electron*

Spectroscopy and Related Phenomena, vol. 43, no. 2, pp. 97–112, 1987.

[30] M. Aronniemi, J. Sainio, and J. Lahtinen, "Chemical state quantification of iron and chromium oxides using XPS: the effect of the background subtraction method," *Surface Science*, vol. 578, no. 1–3, pp. 108–123, 2005.

[31] T. Yamashita and P. Hayes, "Analysis of XPS spectra of Fe^{2+} and Fe^{3+} ions in oxide materials," *Applied Surface Science*, vol. 254, pp. 2441–2449, 2008.

[32] P. C. J. Graat and M. A. J. Somers, "Simultaneous determination of composition and thickness of thin iron-oxide films from XPS Fe 2p spectra," *Applied Surface Science*, vol. 100-101, pp. 36–40, 1996.

[33] A. Malki, Z. Mekhalif, S. Detriche, G. Fonder, A. Boumaza, and A. Djelloul, "Calcination products of gibbsite studied by X-ray diffraction, XPS and solid-state NMR," *Journal of Solid State Chemistry*, vol. 215, pp. 8–15, 2014.

[34] W. J. Quadakkers, K. Schmidt, H. Gruebmeler, and E. Wallura, "Composition, structure and protective properties of Al_2O_3 scales on iron-based oxide dispersion strengthened alloys," *Materials at High Temperatures*, vol. 10, no. 1, pp. 23–32, 1992.

[35] D. Veys, P. Weisbecker, B. Domenichini, S. Weber, V. Fournée, and J. M. Dubois, "Chemical surface ageing in ambient conditions of an Al–Fe–Cr approximant phase," *Journal of Physics: Condensed Matter*, vol. 19, no. 37, Article ID 376207, 2007.

[36] R. C. Lobb, J. A. Sasse, and H. E. Evans, "Dependence of oxidation behaviour on silicon content of 20%Cr austenitic steels," *Materials Science and Technology*, vol. 5, no. 8, pp. 828–834, 1989.

[37] N. Louet, H. Reveron, and G. Fantozzi, "Sintering behaviour and microstructural evolution of ultrapure α-alumina containing low amounts of SiO_2," *Journal of the European Ceramic Society*, vol. 28, no. 1, pp. 205–215, 2008.

[38] J. Chovanec, D. Galusek, J. Ráhe, and P. Šajgalík, "Low loss alumina dielectrics by aqueous tape casting: the influence of composition on the loss tangent," *Ceramics International*, vol. 38, no. 5, pp. 3747–3755, 2012.

[39] V. V. Ivanov, S. Y. Ivin, A. I. Medvedev, S. N. Paranin, V. R. Khrustov, and A. K. Shtol'tz, "Fabrication of Mg- and Ti-doped submicron-grained alpha-alumina-based ceramics," *Inorganic Materials*, vol. 37, no. 2, pp. 194–201, 2001.

[40] T. L. Barr and S. Seal, "Nature of the use of adventitious carbon as a binding energy standard," *Journal of Vacuum Science and Technology A: Vacuum, Surfaces and Films*, vol. 13, no. 3, pp. 1239–1246, 1995.

[41] S. Ben Amor, G. Baud, M. Jacquet, G. Nansé, P. Fioux, and M. Nardin, "XPS characterization of plasma-treated and alumina-coated PMMA," *Applied Surface Science*, vol. 153, no. 2, pp. 172–183, 2000.